J. Fluid Mech. (2006), *vol.* 563, *pp.* 133–158.
doi:10.1017/S0022112006001042 Printed in the United Kingdom

Deformation and breakup of a non-Newtonian slender drop in an extensional flow: inertial effects and stability

By MOSHE FAVELUKIS[1]†, OLGA M. LAVRENTEVA[2] AND AVINOAM NIR[2]

[1]Department of Chemical and Biomolecular Engineering, National University of Singapore, 10 Kent Ridge Crescent, Singapore 119260

[2]Department of Chemical Engineering, Technion – Israel Institute of Technology, Haifa, 32000 Israel

(Received 27 April 2005 and in revised form 7 February 2006)

We consider the deformation and breakup of a non-Newtonian slender drop in a Newtonian liquid, subject to an axisymmetric extensional flow, and the influence of inertia in the continuous phase. The non-Newtonian fluid inside the drop is described by the simple power-law model and the unsteady deformation of the drop is represented by a single partial differential equation. The steady-state problem is governed by four parameters: the capillary number; the viscosity ratio; the external Reynolds number; and the exponent characterizing the power-law model for the non-Newtonian drop. For Newtonian drops, as inertia increases, drop breakup is facilitated. However, for shear thinning drops, the influence of increasing inertia results first in preventing and then in facilitating drop breakup. Multiple stationary solutions were also found and a stability analysis has been performed in order to distinguish between stable and unstable stationary states.

1. Introduction

The subject of deformation and breakup of a drop suspended in another fluid has been studied extensively because of its importance to many physical processes. High-viscosity liquids such as polymer melts, foods and biological materials are usually processed in rotary equipment under conditions in which the flow contains shear or extensional components. A drop present in these types of flow will be deformed. Under some conditions, highly elongated drops can be obtained and, furthermore, if the strength of the flow exceeds some critical value, the drop will break into two or more fragments.

The deformation of a Newtonian drop in a Newtonian liquid under creeping flow conditions is governed by two dimensionless numbers: the capillary number Ca, the ratio of the external viscous force that tends to deform the drop to the surface tension force that tends to keep the drop spherical; and λ, the ratio of the viscosity of the drop to that of the external fluid. In general, the literature distinguishes between small deformations at $Ca \ll 1$, and large deformations at $Ca \gg 1$ and $\lambda \ll 1$. Reviews by Rallison (1984) and Stone (1994) discuss many applications of this subject.

† Author to whom correspondence should be addressed: chemf@nus.edu.sg.

Taylor (1964) was the first to suggest a theoretical model for the deformation and breakup of a slender drop in an axisymmetric extensional and creeping flow. The theory, which was later refined by Buckmaster (1972, 1973), Acrivos & Lo (1978) and others, shows that the slender Newtonian drop has a parabolic shape with pointed ends. Also, according to the theory, the critical capillary number required for breakup increases as the viscosity ratio decreases. However, for a bubble (an inviscid drop) where $\lambda = 0$, a stable steady shape is always possible, and breakup was not predicted.

Acrivos & Lo (1978) argued that the Reynolds number based on the length of a long and slender drop may be not small, and thus, inertial effects should be taken into account. As a first step, they included the effects of inertia in the fluid outside the drop. The modified theory predicts that, contrary to the creeping flow case, a bubble ($\lambda = 0$) can be broken. They also presented a solution for a slightly viscous drop ($\lambda \neq 0$), which provides the critical extensional rate for burst. The results suggest that the burst of a drop can be enhanced by increasing the Reynolds number. Brady & Acrivos (1982) considered the effects of inertia inside and outside the drop. They found that internal inertia has a relatively weak effect and that the zero-internal-inertia results can be used to predict drop breakup.

A feature common to all the deformation problems of slender drops discussed above is the existence of multiple stationary solutions. For the case of a bubble or a drop in a Newtonian liquid under creeping flow conditions, Acrivos & Lo (1978) performed a linear stability analysis on the dynamic governing equation. By expressing the solution as a linear combination of the steady-state solution plus a small unsteady perturbation together with separation of variables, they were able to distinguish between stable and unstable stationary shapes. The stability analysis for the external inertia case was not reported there, and it will be presented in this work. Following Acrivos & Lo (1978), Hinch (1980) considered the general initial-value problem for the evolution of the shape of a bubble. Subsequently, Sherwood (1984) extended the previous theoretical analyses to the case of a nonlinear flow with extensional components, but without external inertia. His time-dependent studies for the case of a Newtonian drop, reveal the possible existence of different breakup mechanisms.

The discussion above has been limited to large deformations in systems where both the drop and the fluid outside it are Newtonian. In many industrial applications, such as in mixing of polymer blends, this is far from reality. In these processes non-Newtonian effects such as shear thinning and elasticity are exhibited. In recent years, attention was given to cases involving drop deformation in non-Newtonian systems. Unfortunately, the theoretical studies were restricted to small and medium deformations under creeping flow conditions. In two previous studies we have focused primarily on slender bodies deforming in linear extensional flow (Favelukis & Nir 2001; Favelukis, Lavrenteva & Nir 2005). In Favelukis *et al.* (2005), which contains a summary of the literature published on non-Newtonian systems, we presented a study of the deformation and breakup of a non-Newtonian slender drop in a Newtonian liquid in an axisymmetric extensional and creeping flow. The rheology of the drop was described by the simple power-law model with index n. It is well known that a power-law fluid does not exist in the general case. However, this simplified rheological model, which permits analytic manipulations, is useful here in view of the fact that the flow within most of the volume of the slender drop is dominated by shear components where the power-law provides a good description of shear thinning or thickening effects. The report in Favelukis *et al.* (2005) suggests that only shear thinning ($n < 1$) and Newtonian drops ($n = 1$) can exist. It was also found that, similar to the case

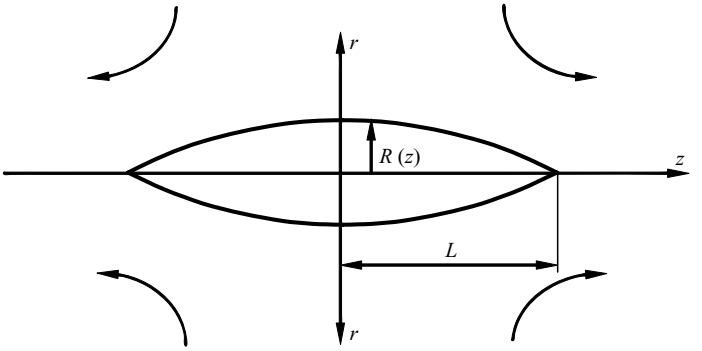

FIGURE 1. A slender drop in a simple extensional flow: $R(z)$ is the local radius and L is the half-length of the drop.

of Newtonian drops, a slender shear thinning drop attains pointed ends. However, Newtonian drops are more elongated than shear thinning drops when subjected to the same flow. Furthermore, the critical capillary number for drop breakup increases as the viscosity ratio decreases and as the power-law index (n) decreases.

In the present paper, we extend our previous theoretical analysis (Favelukis *et al.* 2005) as follows: (a) inertial effects in the external fluid are included; and (b) a stability analysis of the obtained shapes is performed. We start this report by presenting the unsteady governing equations for both the flow inside and outside the drop, where the simple power-law model is assumed for the non-Newtonian fluid inside the drop. Next, solutions for a bubble and a Newtonian drop, which include external inertial effects, as were reported in the literature (Acrivos & Lo 1978), are revisited. Here, we add several new results to the existing knowledge. We then continue with the deformation and breakup of a non-Newtonian slender drop in a Newtonian liquid in an axisymmetric extensional flow. Specifically, we explore the influence of inertia in the external phase on the breakup of the embedded drop and compare these results with our previous predictions for creeping flow (Favelukis *et al.* 2005). We found that the problem contains multiple solutions; therefore, special attention has been given to a stability analysis in order to distinguish between stable and unstable stationary shapes. Finally, conclusions and recommendations for future work are discussed.

2. The governing equations

2.1. *The flow outside the drop*

Figure 1 describes a slender drop with local radius $R(z)$ and a half-length L positioned in an axisymmetric extensional flow. The velocity components of the undisturbed flow are given in cylindrical coordinates by:

$$v_r = -\tfrac{1}{2}Gr, \quad v_z = Gz, \tag{1}$$

where G is the strength of the flow and will be positive in this work.

Following Acrivos & Lo (1978) the velocity components of the disturbed flow are approximated, for $r \geqslant R$ and $-L \leqslant z \leqslant L$, by:

$$v_r = \frac{R}{r}\frac{\partial R}{\partial t} + G\left[-\frac{r}{2} + \frac{R}{r}\left(\frac{R}{2} + z\frac{\partial R}{\partial z}\right)\right], \quad v_z = Gz. \tag{2}$$

Note that, at this approximation, the axial component of the velocity is not altered by the presence of a slender drop. The radial disturbed velocity is obtained from the continuity equation and the kinematic condition in which the normal component of the surface velocity is set equal to the change of the drop radius with time.

The pressure outside the drop (P_{out}) can be obtained by substituting the velocity profile into the Navier–Stokes equations. If the drop is sufficiently slender ($R/L \ll 1$), then the leading order of the pressure outside the drop is (Acrivos & Lo 1978):

$$P_{out} = -\tfrac{1}{2}\rho G^2 z^2. \tag{3}$$

2.2. *The flow inside the drop*

The incompressible non-Newtonian fluid inside the drop is described by the simple power-law model:

$$\boldsymbol{\tau} = m\left|\sqrt{\tfrac{1}{2}(\dot{\boldsymbol{\gamma}} : \dot{\boldsymbol{\gamma}})}\right|^{n-1}\dot{\boldsymbol{\gamma}}. \tag{4}$$

Here, $\boldsymbol{\tau}$ is the viscous stress tensor, $\dot{\boldsymbol{\gamma}}$ is the rate of deformation tensor and m and n are model parameters. For a Newtonian fluid $n = 1$ and m becomes the Newtonian viscosity. For a shear thinning (pseudoplastic) fluid $n < 1$ while for a shear thickening (dilatant) fluid $n > 1$.

Taylor (1964) approximated the flow inside a slender drop as a Poiseuille flow in a fluid pipe with a pressure gradient and with an axial velocity of Gz at the boundary. Furthermore in view of the finding of Brady & Acrivos (1982), we neglect inertia forces inside the drop. Hence, the velocity profile, for the region $0 \leqslant r \leqslant R$ and $0 \leqslant z \leqslant L$, is readily obtained by combining (2), (4) and the equation of motion to give (Favelukis *et al.* 2005):

$$v_z = Gz - \left(\frac{n}{1+n}\right)\left(\frac{R}{2m}\frac{\partial P_{in}}{\partial z}\right)^{1/n} R\left[1 - \left(\frac{r}{R}\right)^{1+1/n}\right]. \tag{5}$$

The volumetric flow rate through each axial cross-section along the drop can be obtained by integrating the velocity profile (Favelukis *et al.* 2005):

$$Q = \int_0^R v_z 2\pi r \,\mathrm{d}r = \pi R^2\left[Gz - \left(\frac{n}{1+3n}\right)\left(\frac{R}{2m}\frac{\partial P_{in}}{\partial z}\right)^{1/n} R\right]. \tag{6}$$

This quantity is balanced by the rate of volume change, measured from the centre of the drop, at $z = 0$, to that cross-section position:

$$Q = -\pi\frac{\partial}{\partial t}\int_0^z R^2 \,\mathrm{d}z. \tag{7}$$

Note also that, at steady state, the volumetric flow rate vanishes everywhere. Equating the last two rates results in an expression for the pressure profile inside the drop:

$$P_{in} = P_{in}(0,t) + 2wmG^n \int_0^z \frac{1}{R}\left[\frac{z}{R} + \frac{1}{R^3}\frac{\partial}{\partial(Gt)}\int_0^z R^2 \,\mathrm{d}z\right]^n \mathrm{d}z, \tag{8}$$

where:

$$w(n) = \left(\frac{1+3n}{n}\right)^n. \tag{9}$$

Here, P_{in} is the pressure inside the drop and $P_{in}(0,t)$ is the unknown pressure at the centre of the drop. For an incompressible bubble (an inviscid drop), $m = 0$, the pressure inside the bubble is uniform and at steady state it is also constant.

2.3. *The normal stress balance*

A normal stress balance at the surface of the slender drop can be written as follows:

$$P_{in} - P_{out} - \tau_{rr,in} + \tau_{rr,out} = \frac{\sigma}{R}, \tag{10}$$

where σ is the surface tension. The subscripts *in* and *out* denote inside and outside of the drop, respectively. Slender drops are obtained when the viscosity of the drop is much smaller than the viscosity of the liquid. It follows that the normal viscous stress inside the drop can be neglected when compared to the normal viscous stress outside the drop. Furthermore, the normal viscous stress of the Newtonian liquid outside the drop, at the drop surface, can be obtained easily with the help of (2). Hence, a dimensionless form of the normal stress balance reduces to:

$$P(0,t)+2w\lambda\int_0^z \frac{1}{R}\left[\frac{z}{R}+\frac{1}{R^3}\frac{\partial}{\partial t}\int_0^z R^2\,\mathrm{d}z\right]^n \mathrm{d}z+\tfrac{1}{2}Re\,z^2-\frac{2}{R}\frac{\partial R}{\partial t}-2\left(1+\frac{z}{R}\frac{\partial R}{\partial z}\right)=\frac{1}{CaR}. \tag{11}$$

Note that for simplicity we have omitted all subscripts. In (11), and in what follows throughout the paper, the pressure is rendered dimensionless with respect to the characteristic stress outside the drop (μG), where μ is the viscosity of the Newtonian fluid outside the drop, all the lengths with respect to the radius of a sphere of an equal volume (a), and t is scaled by $1/G$. The viscosity ratio, the Reynolds number and the capillary number are defined as follows:

$$\lambda = \frac{mG^{n-1}}{\mu}, \quad Re = \frac{\rho G a^2}{\mu}, \quad Ca = \frac{\mu G a}{\sigma}. \tag{12}$$

Equation (11) must be solved with the following three conditions: an initial drop shape: $R(z,0)$; a vanishing radius at the end of the drop: $R(L,t)=0$ (see figure 1); and the requirement that the volume of the drop be conserved:

$$\int_0^L R^2\,\mathrm{d}z = \tfrac{2}{3}. \tag{13}$$

Following Hinch (1980), a formal expression connecting the pressure at the centre of the drop to the dynamic evolution of the drop shape can be obtain by combining (11), (13) and its vanishing time derivative, whence:

$$P(0,t) = 1 + \frac{\dfrac{1}{Ca}\displaystyle\int_0^L R\,\mathrm{d}z - \frac{Re}{2}\int_0^L R^2 z^2\,\mathrm{d}z - 2w\lambda\int_0^L R^2\left[\int_0^z \frac{1}{R}\left(\frac{z}{R}+\frac{1}{R^3}\frac{\partial}{\partial t}\int_0^z R^2\,\mathrm{d}z\right)^n \mathrm{d}z\right]\mathrm{d}z}{\displaystyle\int_0^L R^2\,\mathrm{d}z}. \tag{14}$$

Note that according to Hinch (1980), the numerical integration of the last equation, for the case of an inviscid drop in creeping flow, becomes unstable if the integral in the denominator is replaced by the value 2/3.

In order to eliminate the unknown internal pressure at the centre of the drop, (11) can be differentiated with respect to z to give:

$$2\frac{\partial^2 R}{\partial z\partial t} - \frac{2}{R}\frac{\partial R}{\partial z}\frac{\partial R}{\partial t} + 2z\frac{\partial^2 R}{\partial z^2} - 2\frac{z}{R}\left(\frac{\partial R}{\partial z}\right)^2 + \left(2-\frac{1}{CaR}\right)\frac{\partial R}{\partial z} - Re\,zR = 2w\lambda\left(\frac{z}{R}+\frac{1}{R^3}\frac{\partial}{\partial t}\int_0^z R^2\,\mathrm{d}z\right)^n. \tag{15}$$

The following considerations are made for steady-state conditions. Equation (10) suggests that the normal viscous stress exerted by the external fluid $O(\mu G)$ must be balanced by the surface tension stress $O(\sigma/R)$ leading to $R \sim O(1/Ca)$. It follows from (13) that $L \sim O(Ca^2)$. All the steady terms on the left-hand side of (15), except the inertia term, are $O(R/L)$ and when they are balanced with the term on the right-hand side, which is $O[\lambda(L/R)^n]$, we obtain $Ca\lambda^{1/[3(1+n)]} \sim O(1)$. On the other hand, when the inertia term, that is $O(ReLR)$, is compared with the other terms we have $CaRe^{1/4} \sim O(1)$. Thus, this order of magnitude consideration suggests that the normalized half-length of the drop L/Ca^2 must be a function of two dimensionless strengths of the flow: $f_1 = CaRe^{1/4}$ and $f_2 = Ca\lambda^{1/[3(1+n)]}$. Furthermore, in order to obtain a slender drop ($R/L \ll 1$) the following conditions must also be met: $Ca^3 \gg 1$, $\lambda^{1/(1+n)} \ll 1$, $\lambda Ca^{3n} \ll 1$, and $ReCa \ll 1$. In terms of the aspect ratio of the drop, $\varepsilon = R/L$, the theory holds for small viscosity ratio $\lambda \sim \varepsilon^{1+n}$, large capillary number $Ca \sim \varepsilon^{-1/3}$, and small Reynolds number $Re \sim \varepsilon^{4/3}$. For a Newtonian drop with $n = 1$, the scaling reduces to those uncovered by Acrivos & Lo (1978).

The above dimensional consideration suggests a definition of the following rescaled variables: $y = RCa$ and $x = z/Ca^2$, both having the order of magnitude of 1, and (15) becomes:

$$2\frac{\partial^2 y}{\partial x \partial t} - \frac{2}{y}\frac{\partial y}{\partial x}\frac{\partial y}{\partial t} + 2x\frac{\partial^2 y}{\partial x^2} - 2\frac{x}{y}\left(\frac{\partial y}{\partial x}\right)^2 + \left(2 - \frac{1}{y}\right)\frac{\partial y}{\partial x} - f_1^4 xy = 2wf_2^{3(n+1)}\left(\frac{x}{y} + \frac{1}{y^3}\frac{\partial}{\partial t}\int_0^x y^2\,\mathrm{d}x\right)^n, \quad (16)$$

with an initial shape $y(x, 0)$ and satisfying:

$$y(x_L) = 0, \quad (17)$$

$$\int_0^{x_L} y^2\,\mathrm{d}x = \tfrac{2}{3}, \quad (18)$$

with $x_L = L/Ca^2$. Note that the above definitions simplify the problem since the governing equation is now a function of three parameters (n, f_1, f_2) instead of four (n, λ, Re, Ca).

At steady state, the time-derivative terms in (16) vanish and the radius at the centre of the drop can be expressed as:

$$y(0) = \frac{1}{2v}, \quad (19)$$

$$v = \tfrac{1}{2}P(0) - 1, \quad (20)$$

and where $P(0)$ is the steady pressure at $x = 0$.

For a stationary drop, $y(x)$ decreases monotonically. Indeed, at the end of the drop $y(x_L) = 0$ and $y(x) > 0$ for $x < x_L$. Hence, $y(x)$ decreases at least in some interval. If it is not a decreasing function everywhere, then at some $x_0 > 0$, $y(x_0)$ achieves a maximum, where $y'(x_0) = 0$ while $y''(x_0) < 0$. However, it follows from (16) that $y''(x) > 0$ as soon as $y'(x) = 0$ and hence an intermediate maximum between $y(0)$ and $y(x_L)$ cannot exist.

Next, the solution for a bubble (an inviscid drop) and a Newtonian drop are revisited (Acrivos & Lo 1978), where we offer a new presentation of the solution in which external inertia is included.

3. A bubble in a Newtonian liquid

For an inviscid drop $\lambda = 0$ and at steady state the pressure inside the bubble is constant. Equations (11) and (20) are combined to give in the scaled variables:

$$x\frac{\mathrm{d}y}{\mathrm{d}x} - \left(\nu + \tfrac{1}{4}f_1^4x^2\right)y = -\tfrac{1}{2}. \tag{21}$$

The solution of (21), subject to the boundary condition (17), is of the form:

$$y = \tfrac{1}{4}\exp\left(\tfrac{1}{8}f_1^4x^2\right)\left[E_{1+\nu/2}\left(\tfrac{1}{8}f_1^4x^2\right) - \left|\frac{x}{x_L}\right|^{\nu} E_{1+\nu/2}\left(\tfrac{1}{8}f_1^4x_L^2\right)\right], \tag{22}$$

where $E_q(x)$ is the exponential integral function defined by:

$$E_q(x) = \int_1^{\infty} \frac{\exp(-xt)}{t^q}\,\mathrm{d}t. \tag{23}$$

The solution in (22) is identical to that given by Acrivos & Lo (1978), but is presented in a slightly different form as they used the generalized incomplete gamma function whereas we use integrals of the form of (23). Under creeping flow conditions, $Re = 0$, $f_1 = 0$, $E_{1+\nu/2}(0) = 2/\nu$, and (22) reduces readily to Buckmaster's (1972) expression:

$$y = \frac{1}{2\nu}\left(1 - \left|\frac{x}{x_L}\right|^{\nu}\right). \tag{24}$$

Substituting the last equation into (18) results in:

$$x_L = \tfrac{4}{3}(\nu + 1)(2\nu + 1). \tag{25}$$

Recall that, by solving the solution near $x \to 0$ and a stability analysis, Acrivos & Lo (1978) showed that only $\nu = 2$ results in a stable shape. Hence, under creeping flow conditions the shape of the bubble is a parabola with pointed ends and with $x_L = 20$.

When the inertia term in the liquid outside the bubble is included, a combination of (22) and (18) is required since for every value of ν there is one value of f_1 and one value of x_L. Following Acrivos & Lo (1978) and their requirement of an analytic solution at $x = 0$, this search can be facilitated by employing the following transformation:

$$\eta = f_1^4x^2 \tag{26}$$

by which (21) and (17) become:

$$2\eta\frac{\mathrm{d}y}{\mathrm{d}\eta} - \left(\nu + \frac{1}{4}\eta\right)y = -\tfrac{1}{2}, \tag{27}$$

$$y(\eta_L) = 0. \tag{28}$$

Here η_L is the value of η at the end of the bubble. Note that the above transformation eliminates the parameter f_1 from the governing equation. Thus for a choice of ν, the solution is marched from $\eta = 0$ where $y = 1/(2\nu)$, until η_L where $y = 0$, and the value of f_1 can be calculated from the volume conservation that attains the form:

$$f_1 = \left(\tfrac{3}{4}\int_0^{\eta_L} y^2\eta^{-1/2}\,\mathrm{d}\eta\right)^{1/2}. \tag{29}$$

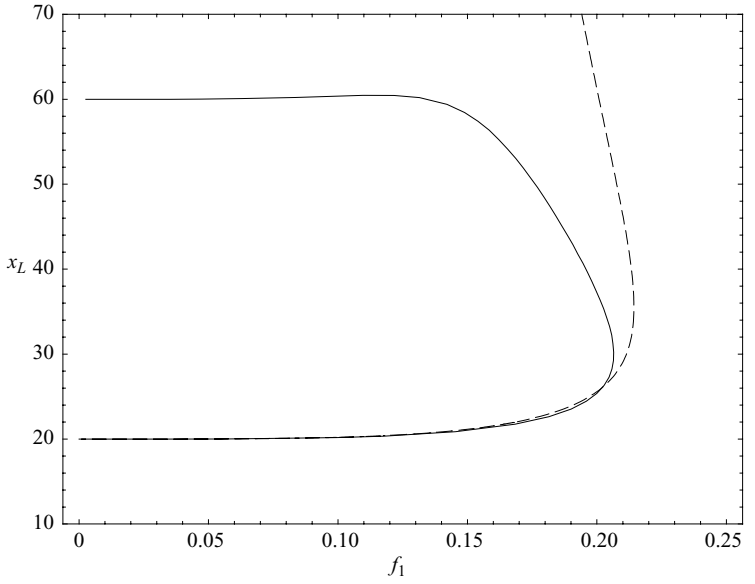

FIGURE 2. The deformation curve of a bubble: the solid line is the exact numerical solution; the dashed line is the approximated analytical solution.

We next follow a procedure applied by Favelukis *et al.* (2005) and express the solution of (27) as a power series in the transformed variable η:

$$y(\eta) = \sum_{k=0}^{\infty} b_k \eta^k \tag{30}$$

where the coefficients are given by:

$$b_k = \frac{(-1)^k}{2^{2k+1} \prod_{j=0}^{k} (\nu - 2j)}. \tag{31}$$

Note that $\nu = 2j$ with $j = 0, 1, 2, 3, \ldots$ are all singular points and the domain of solutions contains several lobes depending on the values of the parameter ν. According to Acrivos & Lo (1978), the first solution is obtained at $2 < \nu < 4$, the next solution is at $6 < \nu < 8$, and so on. The deformation curve of x_L *vs.* f_1 of the first lobe ($2 < \nu < 4$) is plotted in figure 2 (the solid line) where 30 terms were used in (30). We define the term lobe in this work as a line that starts at a specific value of f_1 (or f_2 in § 4) and ν. As the parameter ν increases, the line turns back on itself at a bifurcation turning point and finally, terminates at the original value of f_1 (or f_2). The lobe contains two branches separated by a bifurcation turning point in which f_1 is maximum ($f_{1,max}$). Acrivos & Lo (1978) argued (see also § 7 below) that, along the lower branch, the deformation is stable while the upper branch represents an unstable situation. Thus, the point $f_{1,max}$ is considered as the breakup point. The numerical results suggest that at this point: $\nu = 2.54$, $x_L = 30.0$, and $f_1 = 0.207$. Recall that in the absence of inertia, an inviscid drop does not break. It should be noted that a bubble or a drop does not break as soon as the limit of stability is reached. Once it reaches the limit of stability, a finite amount of time will elapse before breakup can occur.

A relatively simple approximation can be obtained by considering the first two terms of (30) which, together with the condition given by (28), gives:

$$\eta_L \approx 4(\nu - 2), \tag{32}$$

with this result, the dimensionless parameter f_1 can be readily calculated from (29):

$$f_1 \approx \sqrt{\frac{2}{5}} \frac{(\nu - 2)^{1/4}}{\nu}, \tag{33}$$

and the half-length of the bubble is $x_L = 5\nu^2$, a typical result for a parabolic profile.

The breakup point (the maximum value of f_1) can be evaluated from (33). The approximated parameters at the breakup point are $\nu = 8/3 = 2.67$, $x_L = 35.6$ and $f_1 = 0.214$. The deformation curve of the two terms approximation is plotted in figure 2 in the form of a dashed line. Clearly, this approximation is in excellent agreement with the exact numerical results up to the breakup point and deviates from it along the unstable branch.

4. A drop in a Newtonian liquid

We begin this section with preliminary considerations by introducing steady-state asymptotic solutions near the centre and at the end of the drop, and by suggesting a variable transformation to facilitate the solution of (16).

4.1. *Asymptotic expansion near the centre and near the end of the drop*

At the centre of the drop, under steady-state conditions, the radius of the drop is $y(0) = 1/(2\nu)$. Near the centre of the drop ($x \to 0$), we define a small deviation from this value in the form of:

$$\varepsilon(x) = \frac{1}{2\nu} - y(x). \tag{34}$$

Substituting the above definition into the steady (16) and discarding terms that are $O(\varepsilon^2)$ or higher we obtain near the drop centre:

$$-x\frac{\mathrm{d}^2\varepsilon}{\mathrm{d}x^2} + (\nu - 1)\frac{\mathrm{d}\varepsilon}{\mathrm{d}x} - \frac{1}{4\nu} f_1^4 x = 2^n \nu^n w f_2^{3(n+1)} x^n. \tag{35}$$

This last equation can be solved under the condition that $\varepsilon(0) = 0$ to give:

$$\varepsilon = \frac{2^n \nu^n w f_2^{3(1+n)} x^{1+n}}{(1+n)(\nu - n - 1)} + \frac{f_1^4 x^2}{8\nu(\nu - 2)} + C\frac{x^\nu}{\nu}, \tag{36}$$

where C is an integration constant. The slope near the centre of the drop,

$$\frac{\mathrm{d}y}{\mathrm{d}x} = -\frac{2^n \nu^n w f_2^{3(1+n)} x^n}{(\nu - n - 1)} - \frac{f_1^4 x}{4\nu(\nu - 2)} - C x^{\nu - 1}, \tag{37}$$

deserves further attention.

For a Newtonian drop ($n = 1$) we have a singular point at $\nu = 2$. When $\nu > 2$, the last term on the right-hand side of (37) can be neglected compared to the other two terms. Therefore, for $n = 1$, if $\nu > 2$, the slope of y near $x = 0$ is negative. For a non-Newtonian drop, the two singular points are at: $\nu = n + 1$ and $\nu = 2$. If $\nu > n + 1$ and $n < 1$ (shear thinning fluid) the leading term on the right-hand side of (37) is the first one, while if $n > 1$ (shear thickening) the dominant term is the second one. Thus, in either case the slope is negative. This characteristic, for $n < 1$, was found for

drops under creeping flow conditions (Favelukis *et al.* 2005) and it appears that the addition of inertia does not affect it.

Close to the end of the drop ($x \to x_L$), we may assume the following steady radius profile:

$$y = B\left(1 - \frac{x}{x_L}\right)^{\alpha}. \tag{38}$$

Here we define α and B as positive. The three possible cases $\alpha > 1, \alpha = 1$ and $\alpha < 1$ correspond to a cusped end, a pointed end and a rounded end, respectively. Substituting the above expressions into the steady part of (16), results in the following conclusions: for Newtonian and pseudoplastic fluids ($n \leqslant 1$), $\alpha = 1$, and the drop has pointed ends. For shear thickening fluids ($n > 1$) there is no solution. These conclusions are similar to those found in the creeping flow case (Favelukis *et al.* 2005). The leading terms near the end of the drop of the steady (16) are:

$$-2\frac{x}{y}\left(\frac{\mathrm{d}y}{\mathrm{d}x}\right)^2 - \frac{1}{y}\frac{\mathrm{d}y}{\mathrm{d}x} = 2wf_2^{3(n+1)}\left(\frac{x}{y}\right)^n. \tag{39}$$

Note that the inertia term does not contribute to the end shape of the drop. For a Newtonian fluid $n = 1$, all the terms are of the same order of magnitude. For the case $n < 1$, the viscous term in (39) can be neglected as well. Thus, upon solving (39) and (17) we obtain $B = 1/2$ for $n < 1$, and $B = [1 + (1 - \beta_L^2)^{1/2}]/4$ where $\beta_L = 8f_2^3 x_L$ for the case where $n = 1$.

Before ending this section we should note that the slender-body approximation ($R/L \ll 1$) may not be accurate near the stagnation point ($x = 0$) and close to the end of the drop ($x = x_L$). For a detailed discussion, see Favelukis *et al.* (2005).

4.2. *The transformation*

The case of a viscous drop involves a three-dimensional search since every value of v assigns values to each of the parameters f_1, f_2 and x_L. The number of parameters can be reduced using the following transformation (Favelukis *et al.* 2005):

$$\phi = f_2^{3(n+1)} x^{n+1}, \tag{40}$$

and our problem, defined in (16), reduces to:

$$\begin{aligned} &2(n+1)\frac{\partial^2 y}{\partial\phi\,\partial t} - 2(n+1)\frac{1}{y}\frac{\partial y}{\partial\phi}\frac{\partial y}{\partial t} + 2(n+1)^2\phi\frac{\partial^2 y}{\partial\phi^2} - 2(n+1)^2\frac{\phi}{y}\left(\frac{\partial y}{\partial\phi}\right)^2 \\ &\quad + (n+1)\left(2n+2-\frac{1}{y}\right)\frac{\partial y}{\partial\phi} - hy\phi^{(1-n)/(1+n)} \\ &\quad = 2w\phi^{-n/(n+1)}\left[\frac{\phi^{1/(n+1)}}{y} + \frac{1}{(n+1)}\frac{1}{y^3}\frac{\partial}{\partial t}\int_0^{\phi} y^2\phi^{-n/(n+1)}\,\mathrm{d}\phi\right]^n, \end{aligned} \tag{41}$$

subject to the initial shape $y(\phi, 0)$ (or (19) at steady-state), the conservation of volume, (18), and:

$$y(\phi_L) = 0. \tag{42}$$

Here the dimensionless parameter h, characterizing inertia, is defined as:

$$h = \frac{f_1^4}{f_2^6} = \frac{Re}{Ca^2\lambda^{2/(n+1)}}. \tag{43}$$

With this transformation, the governing equation (41) is a function of two parameters (h, n) instead of three (f_1, f_2, n) as in (16). For each choice of h,

h	ν	f_1	f_2	x_L
0	2.4	0	0.148	28.8
1	2.40	0.0568	0.148	28.8
10	2.41	0.0997	0.146	28.9
100	2.44	0.160	0.137	29.0
1000	2.51	0.198	0.107	29.7
∞	2.54	0.207	0	30.0

TABLE 1. Exact parameters at breakup point for a bubble and a Newtonian drop.

the volume conservation can be calculated from (18) and (40) to give:

$$f_2 = \left[\frac{3}{2(n+1)}\int_0^{\phi_L} y^2\phi^{-n/(n+1)}\,\mathrm{d}\phi\right]^{1/3}. \tag{44}$$

Under steady-state conditions, the mathematical procedure described in this section allow us to obtain, for a specific value of h, a numerical solution where the only guess is the parameter ν. The parameter h spans a wide domain where $h \to 0$ is the creeping flow limit while $h \to \infty$ denotes the case of an inviscid drop.

5. A Newtonian drop in a Newtonian liquid

For a Newtonian drop ($n = 1$) in a Newtonian liquid under steady-state conditions, (41) reduces to:

$$8\phi\frac{\mathrm{d}^2y}{\mathrm{d}\phi^2} - 8\frac{\phi}{y}\left(\frac{\mathrm{d}y}{\mathrm{d}\phi}\right)^2 + 2\left(4 - \frac{1}{y}\right)\frac{\mathrm{d}y}{\mathrm{d}\phi} - hy = \frac{8}{y}, \tag{45}$$

where $h = Re/(Ca^2\lambda)$ and $\phi = f_2^6x^2$. As in the case of a bubble, the solution can be obtained by expressing it as a power series of ϕ:

$$y(\phi) = \sum_{k=0}^{\infty} b_k\phi^k, \tag{46}$$

where the first few coefficients are given by:

$$b_0 = +\frac{1}{2\nu}, \quad b_1 = -\frac{(h+32\nu^2)}{8\nu(\nu-2)}, \quad b_2 = +\frac{h(h+32\nu^2)}{32\nu(\nu-2)(\nu-4)},$$
$$b_3 = -\frac{h(h+32\nu^2)(3h+32\nu^2)}{384\nu(\nu-2)(\nu-4)(\nu-6)},$$

and the general recurrence relation for these coefficient is:

$$b_j = \frac{\nu}{2j(\nu-2j)}\sum_{k=0}^{j-1}[8(2k-j)kb_{j-k} - hb_{j-k-1}]b_k \quad (j \geqslant 2). \tag{47}$$

The singular points at $\nu = 0, 2, 4, 6, \ldots$ suggest the existence of multiple lobe solutions. The deformation curve of x_L *vs.* f_2 for various values of h and for the first lobe ($2 < \nu < 4$) is plotted in figure 3(a) where 15 terms were used in (46). A summary of the numerical results, at the bifurcation turning point (breakup point), is given in table 1. We find that as the contribution of external inertia increases, $f_{2,max}$ decreases, and drop breakup is enhanced.

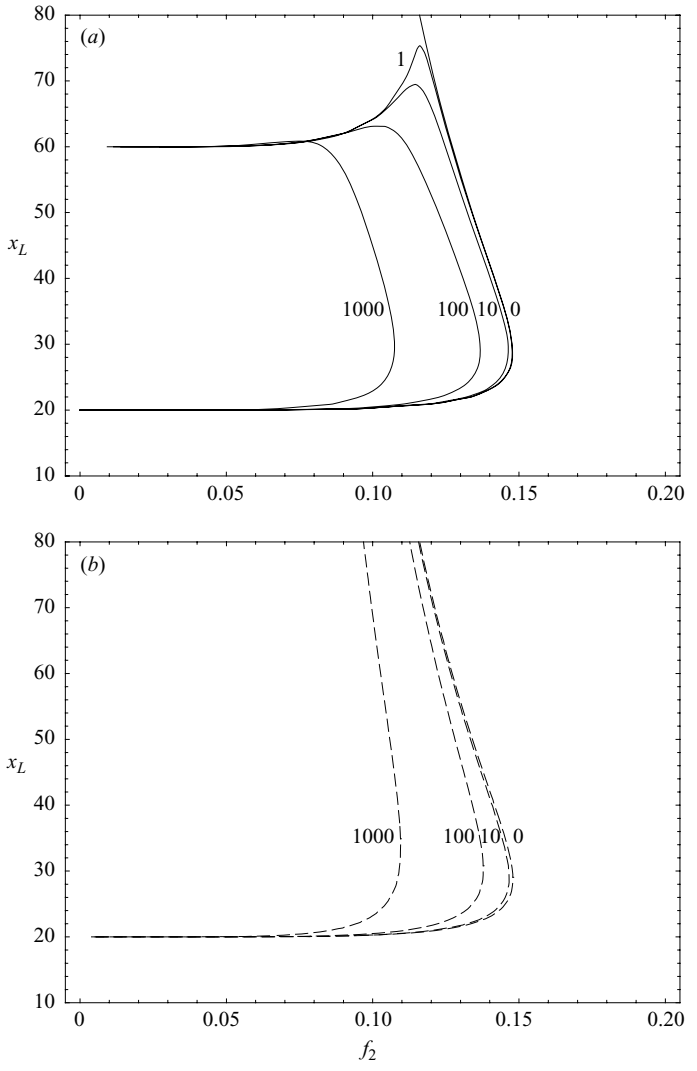

FIGURE 3. Deformation curves of a Newtonian drop, for different values of h: (a) is the exact numerical solution; (b) is the approximated analytical solution.

As in the case of a bubble, a useful approximation can be obtained by considering the first two terms of (46) which, together with the condition given by (42) result in:

$$\phi_L \approx \frac{4(\nu - 2)}{h + 32\nu^2}. \tag{48}$$

From (44), we obtain:

$$f_2 \approx \left(\frac{2}{5}\right)^{1/3} \nu^{-2/3} \left(\frac{\nu - 2}{h + 32\nu^2}\right)^{1/6}, \tag{49}$$

and by incorporating the last two equations into (40), the half-length of the drop is found to be $x_L = 5\nu^2$, which is a typical result for a parabolic profile.

h	ν	f_1	f_2	x_L
0	2.4	0	0.148	28.8
1	2.40	0.0568	0.148	28.8
10	2.41	0.0998	0.147	29.0
100	2.46	0.162	0.138	30.3
1000	2.60	0.204	0.110	33.7
∞	2.67	0.214	0	35.6

TABLE 2. Approximated parameters at breakup point for a bubble and a Newtonian drop.

The breakup point (the maximum value of f_2) can be obtained from (49). The asymptotic cases are:

$$(\nu)_{h\to 0} = 2.4 + 0.000868h, \tag{50}$$

$$(\nu)_{h\to\infty} = 2.67 - \frac{101}{h}. \tag{51}$$

We conclude that the approximate value of ν, at the breakup point, is in the range of 2.4–2.67, and it is not very sensitive to the values of h. For comparison, the exact values are 2.4 (for a drop in creeping flow) and 2.54 (for a bubble with inertia). The approximate solution is plotted in figure 3(*b*) (the dashed lines). It suggests an excellent agreement with the exact numerical results up to the bifurcation turning point (breakup point), see also tables 1 and 2. It should be born in mind that under creeping flow conditions where $h = 0$, the $O(\phi)$ result is actually the exact result.

The approximate values of f_2 at the breakup point are obtained by combining (50) and (51) with (49). Hence:

$$(f_{2,max})_{h\to 0} = 0.148 - 0.000134h, \tag{52}$$

$$(f_{2,max})_{h\to\infty} = \frac{0.358}{h^{1/6}} - \frac{13.6}{h^{7/6}}. \tag{53}$$

We find that, $0 \leqslant f_{2,max} \leqslant 0.148$, where the upper limit corresponds to a drop under creeping flow conditions ($h = 0$), and as the inertia contribution (or h) increases, $f_{2,max}$, decreases. Thus, once again, external inertia tends to facilitate the breakup of the drop.

6. A non-Newtonian drop in a Newtonian liquid

The steady-state shape of a non-Newtonian drop in a Newtonian liquid can be obtained from (41):

$$2(n+1)^2\phi\frac{\mathrm{d}^2y}{\mathrm{d}\phi^2} - 2(n+1)^2\frac{\phi}{y}\left(\frac{\mathrm{d}y}{\mathrm{d}\phi}\right)^2 + (n+1)\left(2n+2-\frac{1}{y}\right)\frac{\mathrm{d}y}{\mathrm{d}\phi} - hy\phi^{(1-n)/(1+n)} = \frac{2w}{y^n}. \tag{54}$$

Two approaches were used to solve this governing differential equation. The first one expresses the solution as an analytic power series expansion about the centre of the drop. The accuracy of this solution depends on the number of terms used, and close to the break-up point we found that this solution became less accurate (especially near the end of the drop). The second approach employs a straightforward two-point

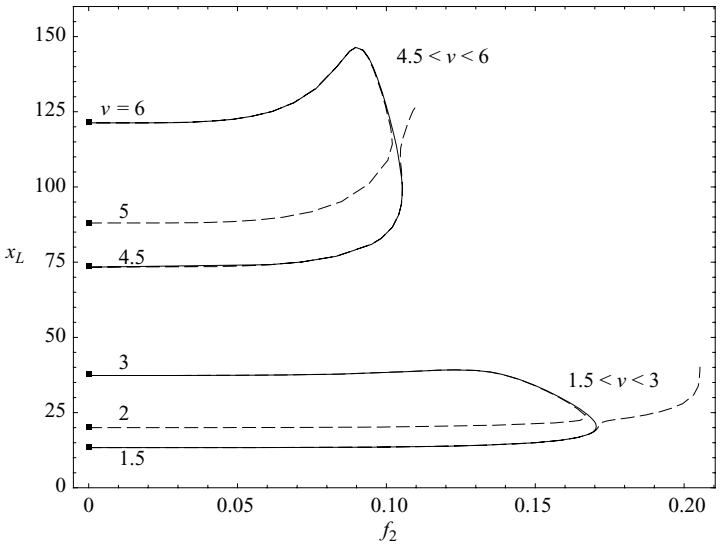

FIGURE 4. Deformation curves of a non-Newtonian drop, for the case $n = 0.5$. The solid line is the case $h = 0$ and the dashed line is the case $h = 1$.

BVP procedure for the nonlinear equation. In both approaches the asymptotically calculated data (see § 4.1) must be satisfied and the volume must be conserved.

Under creeping flow conditions ($h = 0$), the solution to (54) can, thus, be expressed as a power series in ϕ (see (46)). The coefficients which are given in Favelukis *et al.* (2005), suggest singular points at $v = j(n+1)$ with $j = 1, 2, 3, \ldots$ and, similar to the previous cases discussed above, multiple lobes of solutions were found. The first lobe is obtained at $(n+1) < v < 2(n+1)$, the next solution at $3(n+1) < v < 4(n+1)$, and so on.

The deformation curves of x_L *vs.* f_2 of the first two lobes, in the creeping flow case, is shown by the solid lines in figure 4 for the case $n = 0.5$. The dashed curves show the additional branches that results from inertia, at $h = 1$, for comparison. Each solid lobe contains two branches separated by a bifurcation turning point at which f_2 is maximum ($f_{2,max}$). In Favelukis *et al.* (2005) it was shown that, for the case of creeping flow ($h = 0$), at the turning point of the lowest lobe the global maximum of f_2 is achieved, i.e. no stationary solution exists at a larger f_2. It was assumed that under such conditions the drop will eventually break up, and the point where f_2 attains a maximum was referred to as the breakup point. It was assumed also that the deformation is stable along the lower branch of the lowest lobe while the other branches represent unstable configurations. These assumptions were inferred in Favelukis *et al.* (2005) from the analysis of Acrivos & Lo (1978) for the Newtonian drop, but were not proved there. In § 7, we demonstrate via a linear stability analysis that these assumptions were in fact correct.

The report in Favelukis *et al.* (2005) contains also some approximations which can be very useful for fast estimations. Some practical expressions for the breakup point, in the range $0.25 \leqslant n \leqslant 1$, are:

$$f_{2,max} = Ca\lambda^{[1/3(1+n)]} = 0.148 + 0.0454(1-n), \tag{55}$$

$$x_L = 28.8 - 16.4(1-n). \tag{56}$$

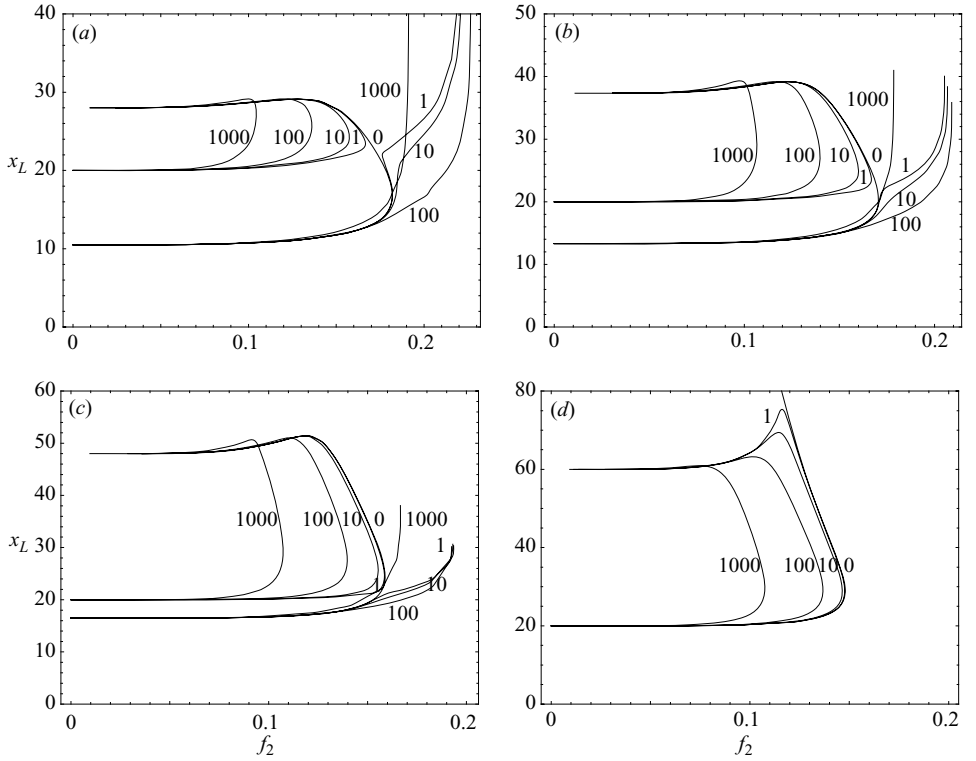

FIGURE 5. Deformation curves of Newtonian and non-Newtonian drops, for different values of h: (*a*) $n=0.25$, (*b*) $n=0.50$, (*c*) $n=0.75$ and (*d*) $n=1$.

Next we turn to the influence of external inertia, $h\neq 0$, at steady state. Since the solution to (54) can no longer be expressed as integer power series in ϕ, we introduce a double series expansion, for $n\neq 1$, of the form of:

$$y(\phi)=\sum_{k=0}^{\infty}(b_k\phi^k+c_k\phi^{kp}). \tag{57}$$

When $h=0$, the creeping flow solution presented in Favelukis *et al.* (2005) is recovered. The coefficient p depends on n, and when the power law has a rational exponent, $n=n_1/n_2$, p is constructed as $p=1/(n_1+n_2)$. It is obvious that when kp is zero or an integer, then the appropriate c_k must vanish. According to (34) and (36), the first three coefficients are:

$$b_0=+\frac{1}{2\nu},\quad b_1=-\frac{2^n\nu^n w}{(1+n)(\nu-n-1)},\quad c_{2n_2}=-\frac{h}{8\nu(\nu-2)}. \tag{58}$$

The coefficients b_k and c_k have many singular points and the first three in ascending order are: $\nu=(n+1)$, $\nu=2$ and $\nu=2(n+1)$.

For $h>0$, the map of branches of the solutions to (54) becomes more complicated as is illustrated in figure 5 for various values of n. It contains families of lobes in which f_2 attains a bifurcation turning point for each choice of h, and the family of lobes is preceded by a family of one-sided bifurcating and h dependent solutions in which x_L increases until a solution can no longer be attained (open curves). Although in the figure we depict deformation curves of x_L *vs.* f_2 only for the range $(n+1)<\nu<$

$2(n+1)$, the pattern is repeated in higher lobes as well, as was previously seen in figure 4. The open curves contain the solution for $(n+1) < \nu < 2$ while the lobe shaped curves span the range of $2 < \nu < 2(n+1)$ for each choice of h. The merged case at $h = 0$ (also shown in the figure) separates the two families. The unique case where $n = 1$, is also shown in the figure for comparison.

The open curves have an S-like shape at small h (see e.g. $h = 1$ curve in figure 5*a*), first going along the $h = 0$ curve repeating its turning point at almost the same f_2 and turning once more afterwards. Thus at some interval of parameter three different solutions, having the same value of f_2 corresponding to the open branch, can be found. These S-shaped curves are typical for systems with hysteresis and we discuss the possibility of the existence of this phenomenon below. Note that in contrast to f_2, the values of parameter ν grow monotonically along each curve in figure 5 and it is, thus, convenient to use this parameter to characterize a point on the curve.

Another unusual feature of the open curves is that they apparently stop at some point corresponding to $\nu < 2$. In the vicinity of this point, however, sharp increases of x_L are encountered with vanishing small changes in f_2 and the drop becomes highly elongated. There are two possibilities: either the curve has a vertical asymptote ($x_L \to \infty$), or it simply stops at some critical elongation having a vertical slope at that point. At this moment, our results cannot distinguish between these two cases. Nevertheless, the existence of critical values of ν and f_2 beyond which the solution cannot be continued is obvious. Furthermore, these are intimately close to the ones where our computations stop, since at this point the slope of the curve is already extremely high. This value will be addressed as a breakup point in the cases when the stability analysis shows that the solution is stable for any lower f_2 (at large values of h).

We shall demonstrate below via a linear stability analysis that only the first open family of solutions has a stable branch in the range $(n+1) < \nu < 2$. These solutions become unstable or cease to exist at some $\nu < 2$. Furthermore, all other solutions, lobes and open branches, appear to be linearly unstable. Figure 6 shows steady-state (stable and unstable) drop shapes, for the case $n = 0.5$ and $h = 1$. The shapes cover both the open branch and the closed lobe of the first family of solutions.

The results presented in figure 5 are somewhat similar to the close problem of drop deformation in an external electrical field (Sherwood 1988; Basaran & Scriven 1989). A drop in an electric field exhibits some of the behaviours found in our work such as stable and unstable stationary solutions and the possibility of hysteresis which will be discussed later on. Similarities and differences in the shapes of the drops in an electrical field and in viscous flow are further addressed in the conclusion section.

7. The stability of the solution

In order to find the range of ν where stable solutions are located we follow Acrivos & Lo (1978) and analyse the stability to small disturbances of the shapes calculated above for bubbles and drops.

7.1. *A bubble in a Newtonian liquid*

For the case of a bubble ($f_2 = 0$), the dynamics is described by the transformed form of (16):

$$4\frac{\partial^2 y}{\partial \eta \partial t} - \frac{4}{y}\frac{\partial y}{\partial \eta}\frac{\partial y}{\partial t} + 8\eta\frac{\partial^2 y}{\partial \eta^2} - 8\frac{\eta}{y}\left(\frac{\partial y}{\partial \eta}\right)^2 + 2\left(4 - \frac{1}{y}\right)\frac{\partial y}{\partial \eta} - y = 0. \qquad (59)$$

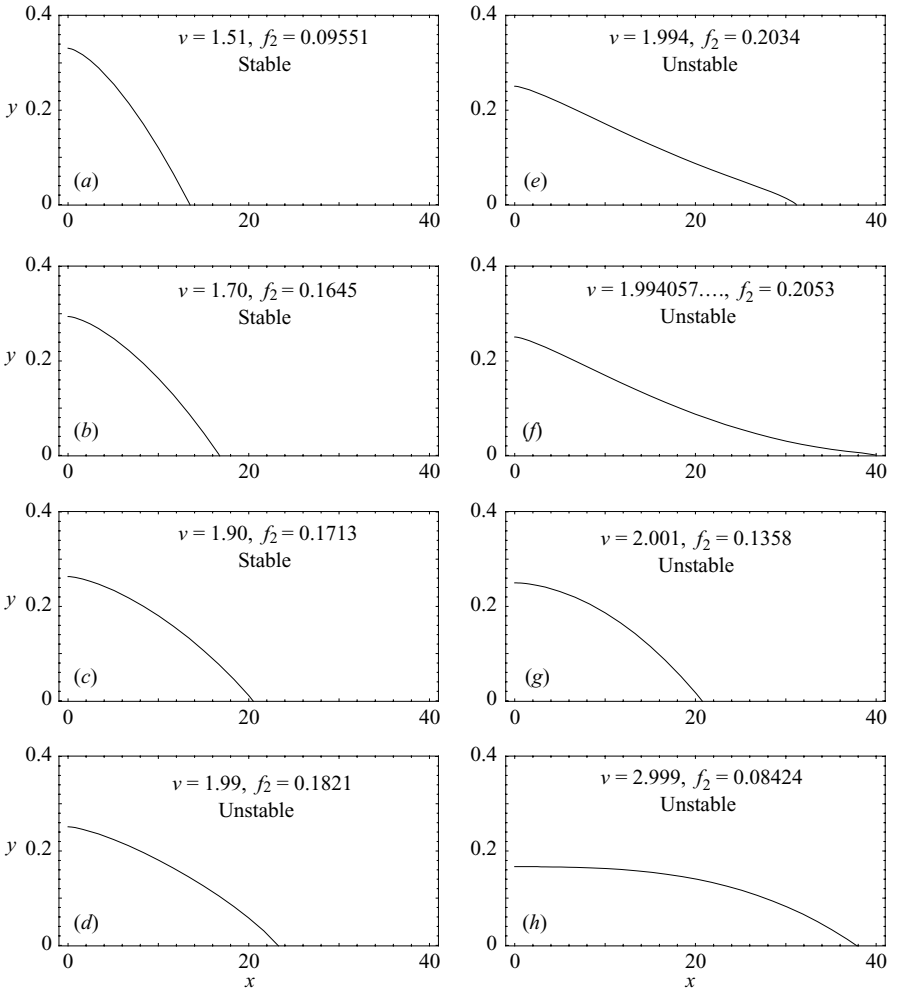

FIGURE 6. Steady-state (stable and unstable) drop shapes, for the case $n = 0.5$ and $h = 1$, of the first family of solutions. (*a*)–(*f*): open branch; (*g*)–(*h*): lobe.

Let

$$y(\eta, t) = y_0(\eta) + y_1(\eta, t), \tag{60}$$

where y_0 is the steady solution and y_1 is a small axisymmetric perturbation from the steady shape ($y_1 \ll y_0$). Combining (59) and (60) and keeping only terms of $O(y_1)$ result in the linear homogeneous equation for y_1:

$$4\frac{\partial^2 y_1}{\partial\eta\partial t} - \frac{4}{y_0}\frac{\mathrm{d}y_0}{\mathrm{d}\eta}\frac{\partial y_1}{\partial t} + 8\eta\frac{\partial^2 y_1}{\partial\eta^2} + 2\left(4 - \frac{1}{y_0} - 8\frac{\eta}{y_0}\frac{\mathrm{d}y_0}{\mathrm{d}\eta}\right)\frac{\partial y_1}{\partial\eta} + \left[8\frac{\eta}{y_0^2}\left(\frac{\mathrm{d}y_0}{\mathrm{d}\eta}\right)^2 + \frac{2}{y_0^2}\frac{\mathrm{d}y_0}{\mathrm{d}\eta} - 1\right]y_1 = 0, \tag{61}$$

which, upon setting $y_1 = g(\eta)\exp(\delta t)$, becomes:

$$8\eta\frac{\mathrm{d}^2 g}{\mathrm{d}\eta^2} + 2\left(4 + 2\delta - \frac{1}{y_0} - 8\frac{\eta}{y_0}\frac{\mathrm{d}y_0}{\mathrm{d}\eta}\right)\frac{\mathrm{d}g}{\mathrm{d}\eta} + \left[\left(4\frac{\eta}{y_0}\frac{\mathrm{d}y_0}{\mathrm{d}\eta} + \frac{1}{y_0} - 2\delta\right)\frac{2}{y_0}\frac{\mathrm{d}y_0}{\mathrm{d}\eta} - 1\right]g = 0. \tag{62}$$

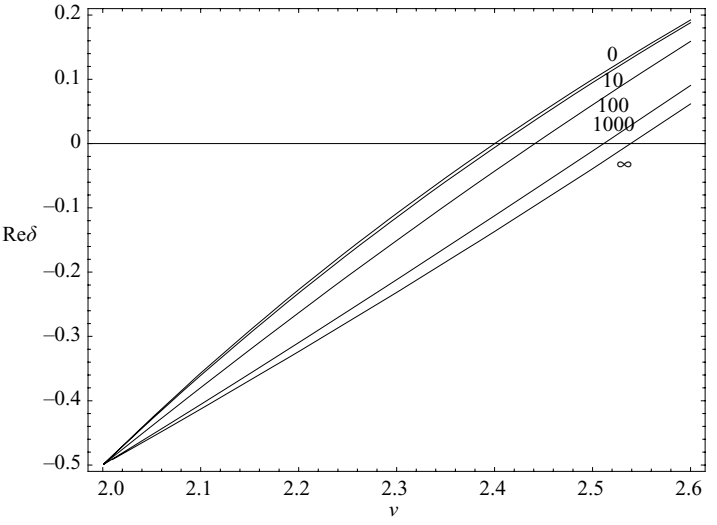

FIGURE 7. The stability of the solution of a bubble and a Newtonian drop, for different values of h.

The solution to (62) is represented as a power series:

$$g(\eta) = \sum_{k=0}^{\infty} d_k \eta^k, \tag{63}$$

where we set $d_0 = 1$ without loss of generality. Finally, the conservation of volume, given by (18), requires, upon differentiation with respect to time, that

$$\int_0^{x_L} y_0 y_1 \mathrm{d}x = \int_0^{\eta_L} y_0 g \eta^{-1/2} \, \mathrm{d}\eta = 0. \tag{64}$$

The eigenvalues δ are determined from (64). Below we are interested in the eigenvalue δ with the highest real part $\mathrm{Re}\,\delta$, since it determines the large time behaviour of an arbitrarily perturbed drop. When $\mathrm{Re}\,\delta$ is negative, small disturbances decay with time, whereas a positive $\mathrm{Re}\,\delta$ indicates an unstable physical situation. The point where $\mathrm{Re}\,\delta = 0$ separates the regions of stability and instability in the parametric space. Again, it can be anticipated that unstable drops will eventually break up and we, therefore, address the points where $\mathrm{Re}\,\delta = 0$ as breakup points.

In figure 7, we have plotted the value of $\mathrm{Re}\,\delta$ as a function of the parameter ν for a bubble and for a Newtonian drop. Note that in these cases δ is real. The case relevant to the bubble is depicted as the curve $h = \infty$. As expected, negative values of δ (stable solutions) are obtained in the range: $2 < \nu < 2.54$, and positive values of δ (unstable solutions) are obtained when $2.54 < \nu < 4$. Thus, our linear stability analysis confirms the argument in Acrivos & Lo (1978) that the bifurcation turning point $\nu = 2.54$, where f_1 obtains its maximum value, is the breakup point. It should be noted that δ was found to be positive for all other lobes of branches having $\nu > 4$ that we have checked and thus no other stable shapes having a larger x_L are expected.

7.2. *A drop in a Newtonian liquid*

With a procedure similar to the one used in the case of a bubble, but employing the transformation in (40), (41) results in the linear equation for the small disturbance y_1:

$$2(n+1)\frac{\partial^2 y_1}{\partial\phi\partial t} - 2(n+1)\frac{1}{y_0}\frac{\mathrm{d}y_0}{\mathrm{d}\phi}\frac{\partial y_1}{\partial t} + 2(n+1)^2\phi\frac{\partial^2 y_1}{\partial\phi^2} - 4(n+1)^2\frac{\phi}{y_0}\frac{\mathrm{d}y_0}{\mathrm{d}\phi}\frac{\partial y_1}{\partial\phi}$$
$$+2(n+1)^2\frac{\phi y_1}{y_0^2}\left(\frac{\mathrm{d}y_0}{\mathrm{d}\phi}\right)^2 + (n+1)\frac{y_1}{y_0^2}\frac{\mathrm{d}y_0}{\mathrm{d}\phi} + (n+1)\left(2n+2-\frac{1}{y_0}\right)\frac{\partial y_1}{\partial\phi} - hy_1\phi^{(1-n)/(1+n)}$$
$$= \frac{2w}{y_0^n}\left[-\frac{ny_1}{y_0} + \frac{2n}{(n+1)}\frac{\phi^{-1/(n+1)}}{y_0^2}\frac{\partial}{\partial t}\int_0^\phi y_0 y_1\phi^{-n/(n+1)}\,\mathrm{d}\phi\right], \tag{65}$$

which, by setting $y_1 = g(\phi)\exp(\delta t)$ is transformed into:

$$2(n+1)^2\phi\frac{\mathrm{d}^2 g}{\mathrm{d}\phi^2} + (n+1)\left[2n+2-\frac{1}{y_0}+2\delta-4(n+1)\frac{\phi}{y_0}\frac{\mathrm{d}y_0}{\mathrm{d}\phi}\right]\frac{\mathrm{d}g}{\mathrm{d}\phi}$$
$$+\left[(n+1)\frac{1}{y_0}\left(\frac{1}{y_0}-2\delta\right)\frac{\mathrm{d}y_0}{\mathrm{d}\phi} + 2(n+1)^2\frac{\phi}{y_0^2}\left(\frac{\mathrm{d}y_0}{\mathrm{d}\phi}\right)^2 - h\phi^{(1-n)/(1+n)} + \frac{2wn}{y_0^{n+1}}\right]g$$
$$= \frac{4wn\delta}{(n+1)}\frac{\phi^{-1/(n+1)}}{y_0^{2+n}}\int_0^\phi y_0 g\phi^{-n/(n+1)}\,\mathrm{d}\phi. \tag{66}$$

Here, in view of the expansion of the steady solution (y_0), the required power series is of the form:

$$g(\phi) = \sum_{k=0}^{\infty} d_k\phi^{kp}, \tag{67}$$

where we set $d_0 = 1$ and with p as in (57), except for a Newtonian drop where $p = 1$. The conservation of volume yields:

$$\int_0^{x_L} y_0 y_1\,\mathrm{d}x = \int_0^{\phi_L} y_0 g\phi^{-n/(n+1)}\,\mathrm{d}\phi = 0. \tag{68}$$

The results for a Newtonian drop are presented in figure 7, which shows the value of δ, which is real in this case, as a function of the parameter ν, for different values of h. The linear stability analysis confirms again that the values of ν, at the breakup point where $\delta = 0$, coincide with the values of ν at the bifurcation turning point where f_2 obtain its maximum (see figure 3*a* and table 1).

Figure 8 shows the results for the case of non-Newtonian drops under creeping flow conditions ($h = 0$) at different values of n. Recall that for the case $h = 0$ it was assumed in Favelukis *et al.* (2005), based on the analysis of Acrivos & Lo (1978) for Newtonian drops, that the lower branch of the lowest lobe is stable and that the drops lose stability at the bifurcation turning point when f_2 attains a maximum. The results of this linear stability analysis confirm these assumptions to be correct.

The results presented for non-Newtonian drops at various values of h are shown in figure 9 for two values of n. Our computations reveal that the first eigenvalue is real for small ν up to some critical value ν, above which it acquires a non-zero imaginary part. In figure 9, the solid lines represent δ which possess real values only, while the dashed lines represent real parts of complex eigenvalues δ with a non-zero imaginary part. In figure 5, the lowest branch of the first open family of solutions, located in the range $(n+1) < \nu < 2$, can be classified into two categories: those with (relatively) low values of h, which contain two bifurcation turning points or an inflection point, and

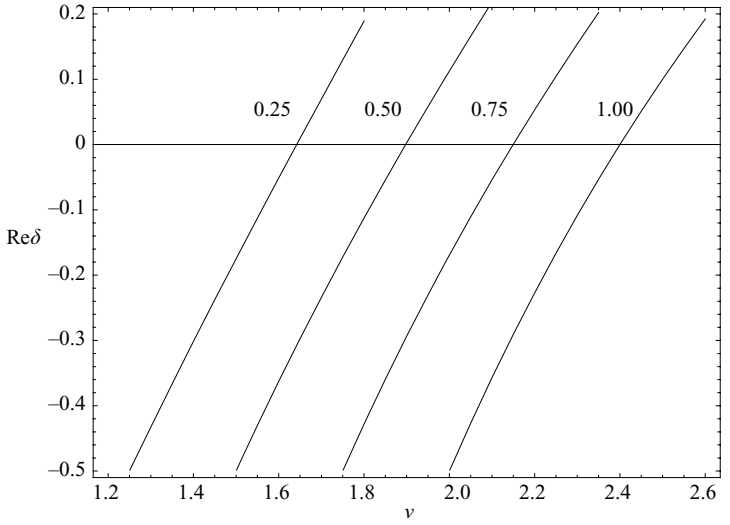

FIGURE 8. The stability of the solution of a non-Newtonian drop under creeping flow conditions ($h = 0$), for different values of n.

those with (relatively) high values of h; having neither turning nor inflection points. From figure 9, we conclude that for low values of h, stable and unstable families of stationary solutions, similar to the results depicted in figures 7 and 8, are separated at the breakup point. On the other hand, at high values of h, we have observed that as long as a solution can be calculated, it was found to be stable. Thus, the point at which a solution can no longer be attained is considered to be the breakup point. It is not clear whether the last observation, at high values of h, reflects a physical transition or is the manifestation of numerical difficulties near the breakup point where the slope in figure 5 becomes infinite. If the curves in figure 5 do not actually stop but do have a vertical asymptote at some f_2, it is natural to expect that the curves in figure 9 do not stop but exhibit a vertical asymptote corresponding to a certain ν. In such a case, the curve will probably intersect the line $\mathrm{Re}\,\delta = 0$ at some breakup point. Nevertheless, as was argued above, the values of ν and f_2 at this point will be close to those obtained at our stop points, and thus provide a good approximation of the breakup criterion. Note that for the case of a non-Newtonian drop with inertia, $\mathrm{Re}\,\delta$ was found to be positive for all other lobes and open branches with $\nu > 2$. Thus, a region of stable solution can be found only along the lowest open branch.

Two other interesting observations can be extracted from figure 9. First, the existence of complex eigenvalues δ with a non-zero imaginary part, suggests the possibility of oscillations, which is often the case in the vicinity of stop points. Thus, the findings in figure 9 for the case of a non-Newtonian drop under the influence of external inertia, may suggest the existence of more than one type of breakup mechanism. Secondly, there exists a region in parametric space where hysteresis is possible. For example, the cases: $n = 0.25$, $h = 8.2$, and $n = 0.50$, $h = 0.28$ are plotted again in figure 10 in the form of the deformation curve, where an enlarged section of the region with two bifurcation turning points is presented.

S-like curves are typical for the classical case of hysteresis, where the lower and upper branches correspond to stable solutions while the intermediate one corresponds to an unstable configuration (see e.g. Sherwood 1988; Wohlhuter & Basaran 1992,

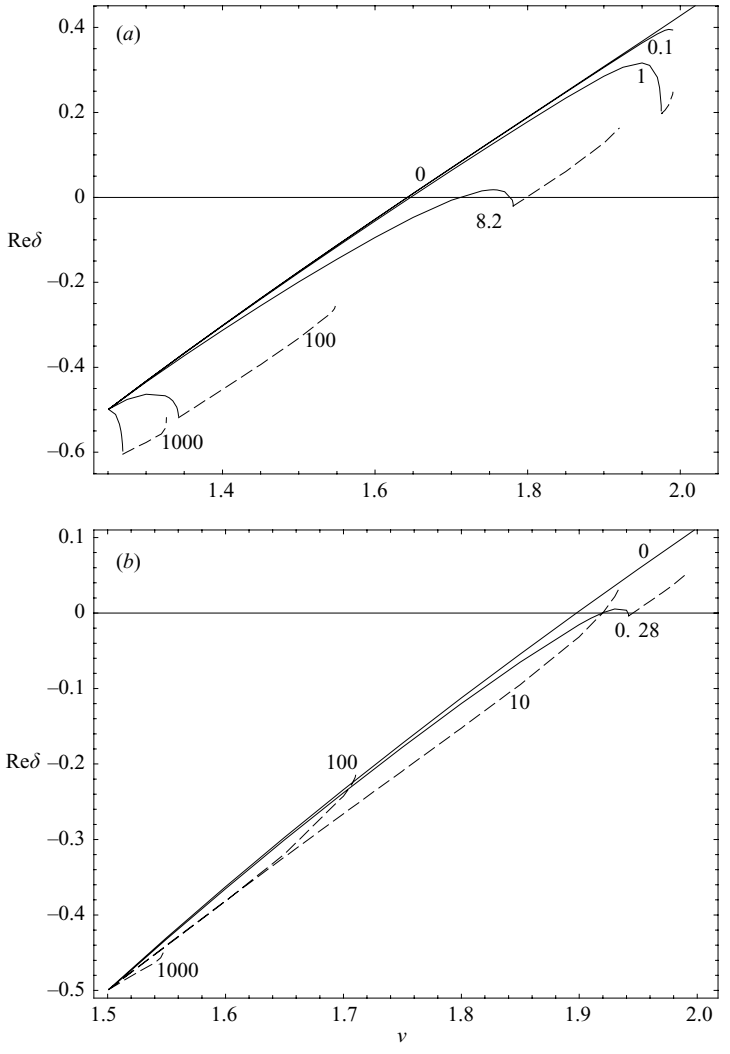

FIGURE 9. The stability of the solution of a non-Newtonian drop, for different values of h. (*a*) $n = 0.25$, (*b*) $n = 0.50$. The solid lines represent real values of δ without an imaginary part; the dashed lines represent real values of δ with an imaginary part.

where this phenomenon is found in a similar problem of deformation of a drop in an electrical field). In this case, when moving along the lower branch by increasing the parameter, upon reaching the first turning point the solution will jump to the upper stable branch. Similarly, on decreasing the parameter along the upper branch down to the second turning point, the solution jumps from the upper branch to the lower one. This presents a complete cycle of hysteresis. In our case, however, the situation is more complicated since the solution is not stable along the entire range of the upper branch.

The solid line in figure 10 corresponds to stable solutions, while the dashed line marks unstable solutions. The solid circle is placed where the imaginary part of δ starts. It is evident that the upper branch loses stability at a value of f_2 that is smaller than that corresponding to the first turning point. Thus, above this value no

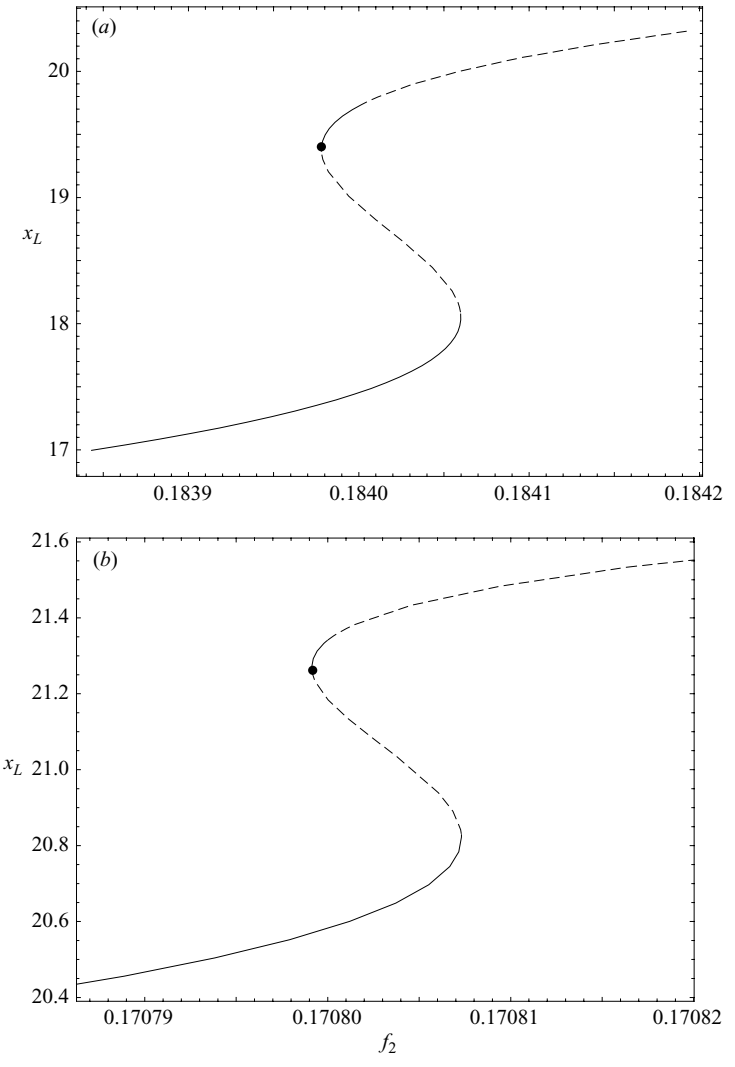

FIGURE 10. Multiplicity in the deformation curve of a non-Newtonian drop. (*a*) $n = 0.25$, $h = 8.2$; (*b*) $n = 0.50$, $h = 0.28$. Stable solutions are depicted by solid curves, while the dashed lines indicate unstable solutions. The solid circle is placed where the imaginary part of δ first appears.

stable solution exists and the drop at a larger f_2 should break up. In this case, it is natural to address the first turning point as the break up criterion. On the other hand, if the solution is chosen at the stable part of the upper branch and the value of the parameter decreases down to and below the second turning point, the solution jumps from the upper branch to the lower one. Thus, we observe the possibility of a non-classical 'one-sided hysteresis'.

Note that for values of h lower than those depicted in figure 10, the S-like form of the deformation curve may appear more pronounced, but the region of stability on the upper branch shrinks and, furthermore, below some critical h it does not exist at all. If, however, the value of h is increased beyond the one depicted in the figure, the value of f_2 at the second turning point approaches that of the first one and the

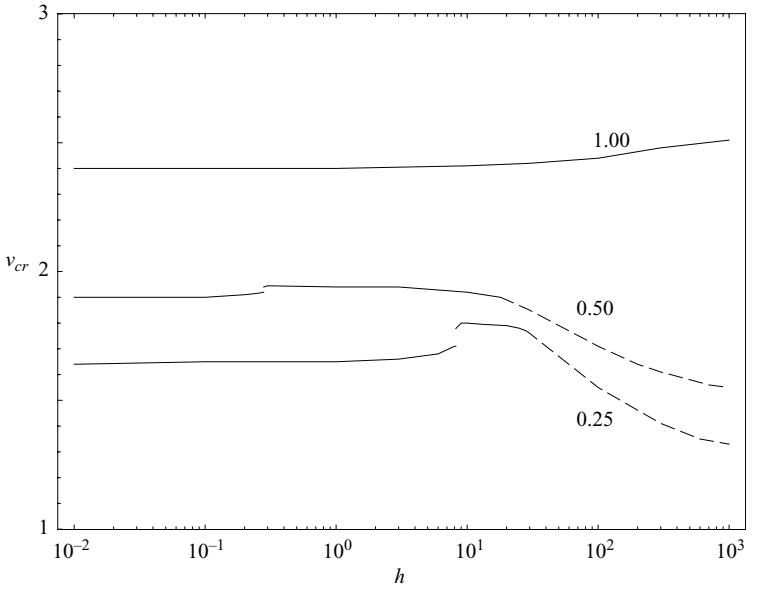

FIGURE 11. The critical value of the parameter v at the breakup point as a function of h, for different values of n. The solid lines represent drops having both stable and unstable stationary solutions in the open branch. The dashed lines represent cases for which only stable stationary solutions were obtained on the open branch.

h	v	f_1	f_2	x_L
0	1.64	0	0.182	16.7
1	1.65	0.0778	0.182	16.8
10	1.80	0.142	0.185	19.8
100	1.59	0.341	0.226	—
1000	1.34	0.470	0.191	—

TABLE 3. Exact parameters at breakup point for a drop with $n = 0.25$.

h	v	f_1	f_2	x_L
0	1.90	0	0.171	20.4
1	1.94	0.0713	0.172	21.4
10	1.92	0.141	0.184	21.9
100	1.73	0.302	0.209	—
1000	1.55	0.424	0.179	—

TABLE 4. Exact parameters at breakup point for a drop with $n = 0.50$.

S-like form of the deformation curve becomes less pronounced. At the same time, the second region of stability on the upper branch is extended and, above some critical value of h, the value of f_2 corresponding to the second loss of stability becomes larger than that of the first turning point. In this case, a classical hysteresis is possible. With the further increase of h, the two turning points merge into an inflection point and above this value the deformation curve is monotonic.

In figure 11 (see also tables 1 to 4), we present the critical value of the parameter v_{cr} corresponding to the first loss of stability as a function of h for different values of the

power law index n. For a Newtonian drop ($n = 1$), as the influence of inertia increases, h increases, v_{cr} slightly increases and f_2 decreases. Hence, the increasing inertia results in obtaining breakup at a lower strength of the flow (f_2). On the other hand, the situation in a shear thinning drop ($n < 1$) is more complicated. While for relatively low h values the loss of stability occurs at the first turning point and the trend in the dependence of v_{cr} on h is as described above, at some critical value of h, which reflects the topological change in the deformation curve mentioned above, v_{cr} jumps to the value corresponding to the second loss of stability. For high h values, the dependence of v_{cr} on h is reversed. Physically, as suggested above, the change in behaviour may indicate that there exist two different competing mechanisms that render the drop shape unstable. Such behaviour was also reported by Sherwood (1984). For some cases, it was found that the drop is pinching at its centre, where $z = 0$, while for other cases the drop showed unrestricted elongation with time and eventual evolution of cusp ends that may indicate the beginning of breakup via pinching. The two (v_{cr}, h) domains in figure 11 are distinguished by solid and dashed lines, respectively. Note also that, contrary to the case of a Newtonian drop, f_2 obtains a maximum value at $h \sim 100$ (See tables 3 and 4). Thus, for shear thinning drops, the influence of increasing inertia results first in preventing, and then in facilitating, drop breakup. Since our stability analysis is linear and only predicts reaction to small disturbances, no prediction of drop breakup mechanism is possible at this stage and it awaits a numerical study of the dynamic drop shape evolution in the various unstable cases.

8. Conclusions

The deformation and breakup of bubbles (inviscid drops), Newtonian drops and non-Newtonian drops in a Newtonian liquid in an axisymmetric extensional flow have been studied theoretically. This paper extends our previous creeping flow analysis (Favelukis *et al.* 2005), by exploring the effects of inertia in the continuous phase, and by performing a stability analysis of the shapes obtained.

The case of a bubble was first treated in the literature by Acrivos & Lo (1978), where they found multiple stationary solutions in the form of many lobes. Each lobe contains two branches separated by a bifurcation turning point. Based on a previous case, they predicted that the lower branch of the first lobe (which describes the lowest possible deformation) is stable while the upper branch and other lobes are unstable. Thus, the turning point is considered as the breakup point. In this work, these results are revisited and confirmed by employing a solution in the form of a power series, and performing a stability analysis to small disturbances. The main result for the case of a bubble is that, contrary to a bubble in a creeping flow, where breakup is not predicted, a small amount of external inertia can cause the bubble to break if the strength of the flow exceeds some critical value.

Next, we considered the influence of inertia on a Newtonian drop, a case that was also first reported by Acrivos & Lo (1978). However, their results do not describe the deformation of the drop, but the breakup criteria only. Here again, the shapes and deformation patterns are presented in the form of a power series. Contrary to the creeping flow solution which contains one lobe, the inclusion of a small amount of external inertia results in many lobes. The stability results are similar to the bubble case, where only shapes predicted along the lowest branch of the first lobe are stable, while other branches and lobes exhibit instability. The main conclusion for the Newtonian case is that as the contribution of external inertia increases, drop breakup is facilitated.

In addition to the exact solutions for the deformation and shapes, we provided two term approximations for the case of a bubble and a Newtonian drop. These are found to be in excellent agreement with the exact results up to the break-up point (point of loss of stability). Since they result in a very simple mathematical expression, without the need for tedious expressions or to perform complicated numerical calculations, they should prove most useful for future fast and practical estimations of steady drop deformations in these cases.

The last case of a non-Newtonian drop is the main contribution of this report. In our creeping flow analysis (Favelukis *et al.* 2005), we reported that only Newtonian and shear thinning drops ($n \leqslant 1$) with pointed ends can exist. Furthermore, we found multiple lobe solutions and, similar to what was suggested by Acrivos & Lo (1978), we assumed there that the stable solution should be located in the lower branch of the first lobe. The analysis in this work reveals that the influence of adding a small amount of external inertia does not change the shape patterns at the end of the drop, but changes dramatically the stability of the steady shapes. The deformation phase plane contains first an open branch and then a lobe, a structure which is repeated. Depending on the amount of inertia, the open branch may contain one or two turning points (less inertia) or even no turning points (more inertia). The stability analysis shows that stable solutions can be found in part of this open branch (less inertia) or along the entire calculated open branch (more inertia). Furthermore, a small region of hysteresis is also predicted.

Hysteresis was found previously by Sherwood (1988) and Wohlhuter & Basaran (1992) in a somewhat similar problem of deformation of a stationary drop in an electrical field, where the shape of the drop is determined by electric and capillary forces. The conservative (potential) nature of both these forces allowed the authors to employ energy consideration and use variational techniques to predict the shape of the drop and to obtain, under certain conditions, a classical cycle of hysteresis. In our case, the competing forces are capillary, viscous and inertial, the latter two being non-conservative, and the hysteresis that we have found is of a more complicated and non-classical nature. Another exciting fact that we have found is that the loss of stability may occur at an imaginary eigenvalue-suggesting the possible existence of oscillatory regimes in the evolution of drop shapes.

We conclude that the effect of increasing inertia on shear thinning non-Newtonian drops results first in preventing and then in facilitating drop breakup. The results presented here lead us to suggest that the influence of inertia results in more than one breakup mechanism, depending on the amount of inertia. This last point will awaits a numerical study of the dynamic drop shape evolution at the various unstable cases.

This research was supported by a grant from the National University of Singapore. A. N. wishes to acknowledge the support from the Department of Chemical and Biomolecular Engineering at NUS during a sabbatical stay. O. M. L. acknowledges the support of the Israel Ministry for Immigrant Absorption.

REFERENCES

Acrivos, A. & Lo, T. S. 1978 Deformation and breakup of a single slender drop in an extensional flow. *J. Fluid. Mech.* **86**, 641–672.

Basaran, O. A. & Scriven, L. E. 1989 Axisymmetric shapes and stability of charged drops in an external electric field. *Phys. Fluids* A **1**, 799–809.

Brady, J. F. & Acrivos, A. 1982 The deformation and breakup of a slender drop in an extensional flow: inertial effects. *J. Fluid Mech.* **115**, 443–451.

Buckmaster, J. D. 1972 Pointed bubbles in slow viscous flow. *J. Fluid. Mech.* **55**, 385–400.

Buckmaster, J. D. 1973 The bursting of pointed drops in slow viscous flow. *J. Appl. Mech.* E **40**, 18–24.

Favelukis, M. & Nir, A. 2001 Deformation of a slender bubble in a non-Newtonian liquid in an extensional flow. *Chem. Engng Sci.* **56**, 4643–4648.

Favelukis, M., Lavrenteva, O. M. & Nir, A. 2005 Deformation and breakup of a non-Newtonian slender drop in an extensional flow. *J. Non-Newtonian Fluid Mech.* **125**, 49–59.

Hinch, E. J. 1980 The evolution of slender inviscid drops in an axisymmetric straining flow. *J. Fluid Mech.* **101**, 545–553.

Rallison, J. M. 1984 The deformation of small viscous drops and bubbles in shear flows. *Annu. Rev. Fluid. Mech.* **16**, 45–66.

Sherwood, J. D. 1984 Tip streaming from slender drops in a nonlinear extensional flow. *J. Fluid Mech.* **144**, 281–295.

Sherwood, J. D. 1988 Breakup of fluid droplets in electric and magnetic fields. *J. Fluid Mech.* **188**, 133-146.

Stone, H. A. 1994 Dynamics of drop deformation and breakup in viscous fluids. *Annu. Rev. Fluid. Mech.* **26**, 65–102.

Taylor, G. I. 1964 Conical free surfaces and fluid interfaces. *Proc. 11th International Congress on Applied Mechanics, Munich*, pp. 790–796. Springer.

Wohlhuter, F. K. & Basaran, O. A. 1992 Shapes and stability of pendant and sessile dielectric drops in an electric field. *J. Fluid Mech.* **235**, 481–510.